The University of South Bohemia in České Budějovice

Faculty of Science

Ultrastructural features of SARS-CoV-2 infection in the lungs

Bachelor thesis

Laboratory of Electron Microscopy

Tereza Kulhánková

Supervisor: Marie Vancová, Ph.D.

Co-supervisor: Tomáš Bílý, Ph.D.

České Budějovice 2023

Kulhánková, T., 2023: Ultrastructural features of SARS-CoV-2 infection in the lungs, Bc. Thesis, in English – 39 p., Faculty of Science, University of South Bohemia, České Budějovice, Czech Republic.

Annotation

The main aim of this bachelor thesis is to investigate the ultrastructural features of SARS-CoV-2 infected lung tissues using TEM. The thesis begins with an introduction to the anatomy of the lung and the characteristics of SARS-CoV-2, including its replication process. The basic tool for this research is transmission electron microscopy (TEM), which is described here in detail, including its main components. In a separate chapter of the bachelor thesis, the sample preparation procedure and the use of the VERO cell line for the study of virus replication are described. The results of these experiments are presented and discussed with emphasis on the specific ultrastructural changes caused by SARS-CoV-2 infection. The final section summarizes the key findings and discusses their implications for our understanding of COVID-19 pathogenesis. This thesis contributes to current SARS-CoV-2 research by providing valuable insight into SARS-CoV-2 infected lung tissue at the ultrastructural level, which may aid in the development of novel therapeutic strategies against this disease.

Declaration

I declare that I am the author of this qualification thesis and that in writing it I have used the sources and literature displayed in the list of used sources only.

Place, date.

České Budějovice, 14th of August 2023.

.....

Acknowledgement

I would like to express my gratitude to my supervisor RNDr. Marie Vancová and my co-supervisor Tomáš Bílý Ph.D. for their great guidance, patience and providing me with all the help they could for me to be able to do this work. A very special thank you goes to RNDr. Marie Vancová, this thesis could not have been possible without her, she was a great supervisor and always helpful. I would also like thank my family, especially my mother for her support and motivation throughout this process. I would also like to thank my friends for being supportive this whole time.

Thank you all very much.

Contents

1. Introduction

1.1. Alveoli

Alveoli play a crucial role as the primary gas exchange units in the lungs, due to their close proximity to the blood capillaries (Hsia et al., 2016; Knudsen & Ochs, 2018). The lung parenchyma, specifically the alveolar region, accounts for approximately 90% of the total lung volume. In contrast, the non-parenchymal portion comprises of larger vessels and conducting airways (Knudsen & Ochs, 2018). These alveoli are lined by a specialized alveolar epithelium known as pneumocytes, which form the air-facing component of the blood-gas barrier. The counterpart of this barrier is the endothelium, facing the capillary lumen. These two layers are separated by an interstitial space with varying composition and thickness (Hsia et al., 2016; Knudsen & Ochs, 2018). The alveolar interstitium contains a delicate network of connective tissue fibers intricately linked with the capillary network (Hsia et al., 2016).

1.1.1Alveolar epithelium

The alveolar epithelium forms a continuous layer that envelops the alveoli and consists of two cell types: pneumocyte type 1 (Pneu1) and pneumocyte type 2 (Pneu2). Pneu1 cells are crucial components of the air-blood barrier, characterized by their thin, branched, squamous appearance. Their cytoplasmic stems ensure a connection to the nucleus despite their delicate branching. These Pneu1 cells cover approximately 95% of the lung alveoli surface, making them the predominant cell type in this region (Hsia et al., 2016; Knudsen & Ochs, 2018; Ochs et al., 2020; Zhao et al., 2010)

The remaining alveolar surface is occupied by interspersed pneumocyte type 2 cells (Zhao et al., 2010). Distinguished by their cuboidal shape and distinctive lamellar bodies, which serve as storage for pulmonary surfactant, Pneu2 cells play a vital role in epithelial renewal and repair (Hsia et al., 2016; Knudsen & Ochs, 2018; Ochs et al., 2020; Zhao et al., 2010). When Pneu1 damage occurs, Pneu2 cells cover the exposed surface and facilitate epithelial restoration through proliferation, migration, and differentiation into Pneu1 cells (Zhao et al., 2010).

Beyond their role in repair and renewal, Pneu2 cells have the ability to modulate inflammatory and oxidative stress responses by providing reducing substances or triggering immune cell responses, such as macrophage and neutrophil activation. They secrete a wide array of cytokines and proteins that contribute to these functions (Ruaro et al., 2021; Zhao et al., 2010).

1.2. SARS-CoV-2

Severe acute respiratory syndrome coronavirus 2, known as SARS-CoV-2, is a positive single stranded RNA virus that belongs to the group of beta coronaviruses (Lai et al., 2020). These viruses are characterized by the presence of a viral envelope around their outer layer, covered with typical spike proteins which are vital in the process of viral entry into host cells (reviewed by Harrison et al., 2020; reviewed by Jackson et al., 2022; reviewed by Perlman & Netland, 2009). Similarly to other RNA viruses, they replicate in the cytoplasm and assemble at intracellular membranes (reviewed by Hopfer et al., 2021).

These viruses are also highly pathogenic, they were the cause of the Covid-19 global pandemic, which begun in the year 2020. The first outbreak, which at the time was registered as cases of pneumonia with an unknown cause, was reported on December 31st, 2019 by the Wuhan Municipal Health Commission in Wuhan, China (Centers for Disease Control and Prevention, 2022). However, by January 2020, there were 40 identified cases. By this time, scientists in Wuhan have obtained the genetic sequence of this atypical pneumonia virus, and according to sequence similarity, it was classified as a Novel Coronavirus by the public health officials in China (Centers for Disease Control and Prevention, 2022). WHO had not yet officially confirmed whether the SARS-CoV-2 virus was transmitted by human-to-human contact, but due to prior knowledge, it was deemed as very likely (Centers for Disease Control and Prevention, 2022). This was later confirmed by Chinese government officials. The virus rapidly spread across China, most of Asia and then the United States, and on January 31st WHO declared a Public Health Emergency of International Concern (Centers for Disease Control and Prevention, 2022). On March 11th 2020, due to the rapidly

escalating situation, and the spread of the virus to Europe as well, a global pandemic was declared (Murgolo et al., 2021).

1.2.1 Variants of SARS-CoV-2

Since the start of the pandemic, numerous variants of SARS-CoV-2 have emerged, most dominant ones being Alpha, Beta, Delta and Omicron. They are natural in the process of virus evolution, however some variants can become of concern as they can become more aggressive, resistant to vaccines and have a higher transmission rate. As the SARS-CoV-2 virus spreads and replicates, it naturally changes over time and modifies genetically, hence the emergence of new variants. Variants have their own specific viral genome that contains one or more changes (genetic mutations) from the original ancestral strain, which can be tracked by genomic sequencing. In this thesis, the alpha variant (B.1.1.7) is further investigated.

1.2.2 Structure of SARS-CoV-2

Corona viruses consist of positive-sense single-stranded RNA. They have the largest genome of all RNA viruses; the genome size of SARS-CoV-2 that was sequenced in 2020 was found to be around 29.9 kb (Lu et al., 2020). The SARS-CoV-2 virions have a spherical shape and their external surface is covered in spike glycoproteins S, which are vital in the process of viral infection. The average diameter of the virus in cross-sections was found to be between 60 and 140 nm (reviewed by Hopfer et al., 2021; Zhu et al., 2020). The main structural proteins are the spike glycoprotein S, transmembrane proteins, membrane protein M, envelope protein E, and the nucleocapsid protein N (reviewed by Harrison et al., 2020; reviewed by Jackson et al., 2022; reviewed by Perlman & Netland, 2009).

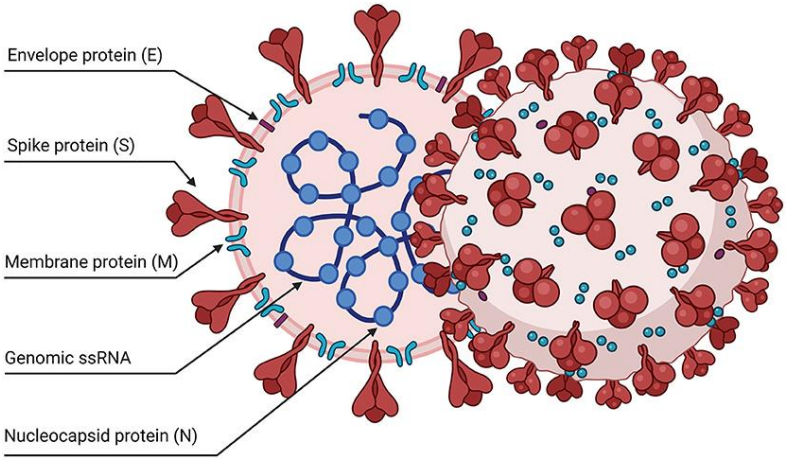

Figure 1: Schematic representation of the SARS-CoV-2 viral particle (Pizzato et al., 2022).

The entry into a host cell is mediated by spike glycoproteins S, which are arranged in homotrimers sticking out from the virions surface (Tortorici & Veesler, 2019). The S protein is made up of two functional subunits S1 and S2 (Walls et al., 2020). The S1 subunit includes the essential receptor binding domain, which initiates the infection and subsequent replication when it binds to a specific receptor on a host cell (Gui et al., 2016; Kirchdoerfer et al., 2016; Pallesen et al., 2017; Song et al., 2018; Walls et al., 2016; Walls et al., 2017; Yuan et al., 2017).

1.2.3. Replication process of SARS-CoV-2

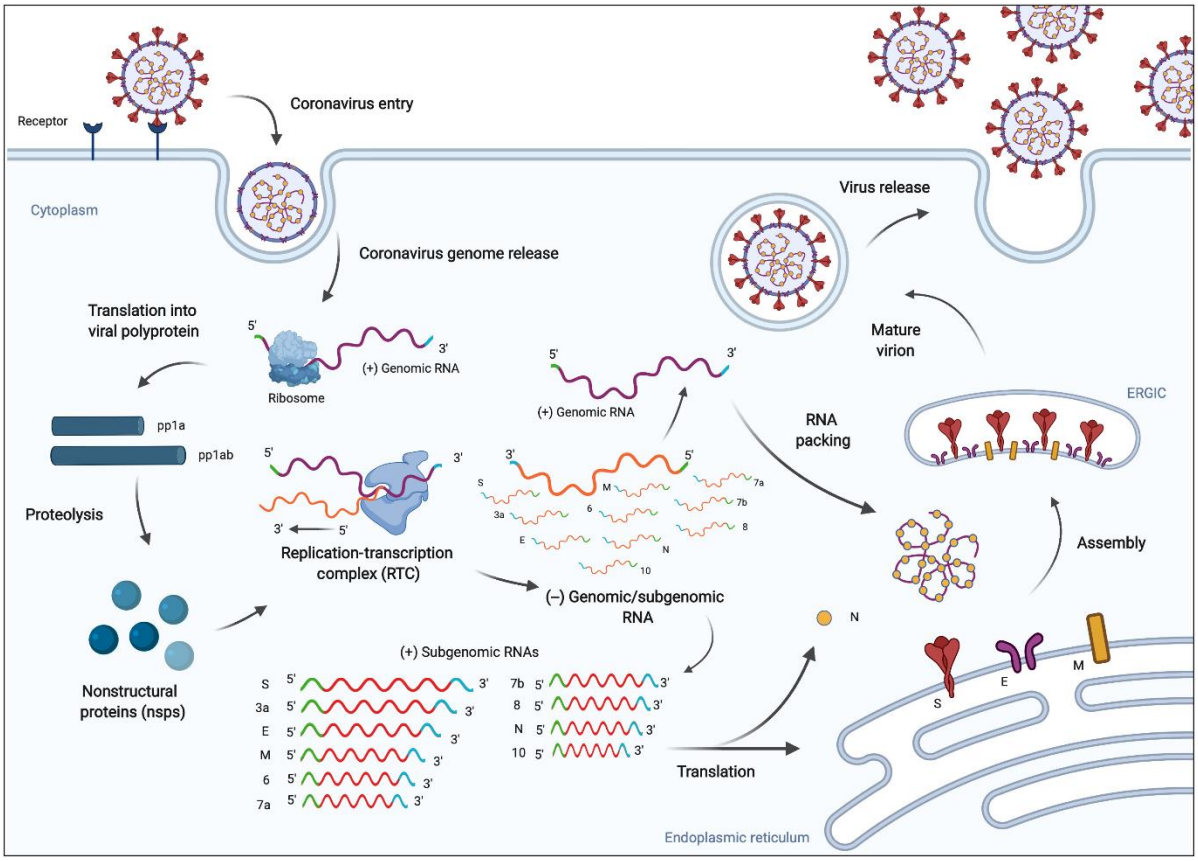

Figure 2: The life cycle and replication process of SARS-CoV-2 **(**Zafferani et al., 2021).

Transmission electron microscopy can be used to observe and better understand the coronavirus replication in cells. The process is illustrated in Figure 2. In the infected cells, SARS-CoV-2 is not located freely within the cytoplasm, but rather as assembled virions inside vacuoles (Goldsmith et al., 2004; reviewed by Hopfer et al., 2021; Zhu et al., 2020). The viral fusion and uptake occur at the ribosomes in the host cell's cytoplasm, where the S protein interacts with the ACE2 receptor (reviewed by Hopfer et al., 2021). After binding to the receptor, cleavage of the S protein triggers early fusion between the viral and endosomal membranes, causing the release of viral RNA into the cytoplasm (reviewed by Hopfer et al., 2021). A serin protease furin is needed for the cleavage to occur. Cleavage can also occur by other proteases, following fusion of the late endosome with a lysosome (reviewed by Hopfer et al., 2021). After the viral genome is released into the cytoplasm, genomic RNA undergoes partial translation of two open reading

frames, ORF1a and ORF1b (Oliveira et al., 2020). The resulting polyproteins are then modified through co-translation and post-translation and packaged into non-structural proteins (V'kovski et al., 2020). These assemble to form the viral replicase translation complex, that is necessary for synthesis of RNA, as well as for replication and transcription of sub-genomic RNA (Fehr & Perlman, 2015). Subsequently, this initiates remodelling of the intracellular membranes that leads to the formation of a three-dimensional 'replication membranous web' (reviewed by Hopfer et al., 2021).

The structural proteins S, M, and E are synthesized from sub-genomic RNA's and inserted into the endoplasmic reticulum, after which they are directed to an intermediate compartment known as the ERGIC, localized between the endoplasmic reticulum and the Golgi apparatus (Oliveira et al., 2020). Viral genomes are enclosed by the N protein and combined with the structural proteins to create virus particles (Fehr & Perlman, 2015; Siu et al., 2008). The M protein is attached to the E protein and subsequently to the nucleocapsid. As the last step of the virion assembly, the S protein is integrated into the virions (Oliveira et al., 2020). After fusion with the cell plasma membrane, the virions in vesicles are released into the extracellular space through exocytosis (reviewed by Hopfer et al., 2021).

Typical for viral replication are double membrane vesicles (DMV) (reviewed by Hopfer et al., 2021). Soon after infection occurs, DMV´s are the initial site of viral RNA replication, as they are the most prominent structure unit of the replication membranous web (reviewed by Hopfer et al., 2021). Their shape is usually round/oval, ranging in size from 200 to 300 nm. They are found arranged in clusters. Inside the DMV's are double-stranded RNA intermediates of viral genome replication and the synthesis of sub-genomic RNA (Wolff et al., 2020).

1.3. VERO cell lineage

The VERO cells are a mammalian cell lineage. They were isolated from kidney epithelial cells that were extracted from an African green monkey. The lineage originally comes from Chiba, Japan, where it was started on March 27th 1962 by Y.Yasumura and Y.Kawakita at the University of Chiba (Osada et al., 2014). It is one of the most commonly used mammalian cell lineages in the world when it comes to research and cultivation (Ammerman et al., 2008). The cells are continuous, meaning they have an abnormal amount of chromosomes, therefore they can be replicated through many cycles of cell division without deteriorating (Osada et al., 2014). They display sensitivity to different viruses, making them ideal for the study of vaccination against viruses or various other pathogens (Osada et al., 2014).

VERO cells are very commonly used in the study of SARS viruses, since the ACE2 receptor is expressed in abundance in them (Gillim-Ross et al., 2004). An important characteristic of VERO E6 cells is their display of contact inhibition upon forming a monolayer, rendering them favourable for cultivating slow-replicating viruses (Pires De Souza et al., 2022). For already 20 years, VERO E6 cells have been widely employed in researching SARS-CoV-like viruses and modelling cell-culture-based infections. This popularity is due to their capacity to support the replication of viruses to significant levels (Pires De Souza et al., 2022). The heightened susceptibility of these cells might be attributed to their elevated expression of the ACE-2 receptor (Gillim-Ross et al., 2004), which is utilized by SARS-CoV as well as by SARS-CoV-2 (Hoffmann et al., 2020).

1.4. Transmission Electron Microscopy

Transmission electron microscopy belongs to the techniques of electron microscopy used to obtain high-resolution images of biological specimens, in order to analyse the ultrastructure and composition of the biological samples (Winey et al., 2014). Transmission electron microscopy uses an accelerated beam of electrons as the source of illumination, which is focused on the sample to form an image which provides ultrastructural information about the specimen (Winey et al., 2014). To allow electrons to pass through the material, a thin specimen or

thin section of the specimen is used in TEM. Several processes take place as the electron beam interacts with the sample, such as scattering.

In scattering, electrons interact strongly and distinctly with matter (Franken et al., 2020). There are two types of scattering: elastic and inelastic scattering (C. Barry Carter & Williams, 1996). Elastic scattering means electrons change direction but keep their energy, while inelastic scattering involves energy exchange between electrons and the sample (Franken et al., 2020). Unlike elastic scattering, inelastic processes are less focused (not as localized) and don't provide high-resolution details (Franken et al., 2020). The identification and location of particular elements within a sample can be done with an energy filter, by detecting the inelastic scattered electrons which form an image via exclusion of electrons from unwanted energies (Kuo, 2014).

The main parts of a transmission electron microscope include the electronics, vacuum part, imaging part and the image recording part (Transmission Electron Microscopy, n.d.). The first part of the microscope is the electron gun, which is necessary to generate and accelerate the electrons (Transmission Electron Microscopy, n.d.). Thermionic emitters operate based on the concept that when a substance is sufficiently heated, electrons will be emitted as their energy surpasses the inherent barrier that confines them (Franken et al., 2020). Electrons can be extracted from a metal either by heating (thermionic guns), or by an electrical field (Field Emission Gun). The TEM JEM-1400 JEOL uses a Lanthanum Hexaboride (LaB_6) cathode as its thermionic source, however it can also operate using the Tungsten one (BIOLOGICKÉ CENTRUM AV ČR, v. v. I. | Mikroskopy a Počítače pro Zpracování Dat, n.d.). In the TEM JEM-1400 JEOL used in this work, the accelerating voltage can reach up to 120 kV.

Typically, a TEM consists of several different types of electromagnetic lenses and apertures; objective aperture, objective lens, diffraction lens, intermediate lens and projector lens (Transmission Electron Microscopy, n.d.). The magnifying and focusing of the electron beam is done by electromagnetic lenses, which work as optical convex lenses. Magnification can be altered by changing the current applied on the lens.

The optical system of TEM consists of condensers, an objective, and an intermediate and projector lens (Transmission Electron Microscopy, n.d.). There are two condensers, one creates the de-magnified image of the gun crossover, and

the other is responsible for the convergence of the beam at the specimen (Subramanian, 2018). The objective generates the first intermediated inverted image, as well as determining the final resolution. The intermediate and projector lens then magnify the image formed by the objective (Subramanian, 2018).

The objective lens is usually a twin lens, composed of upper and lower pole pieces (Subramanian, 2018). They form the image and diffraction pattern. The focusing of the image can be done by changing the current on the objective lens. In transmission electron microscopes, there are several apertures (see Figure 3). Aperture types are condenser apertures, which limit the beam divergence, and objective apertures, which control the contrast in the image (Transmission Electron Microscopy | Central Microscopy Research Facility, 2019). Deflection coils are important for beam alignment, and double deflection coils allow independent beam shift and tilt (Deflector/double-deflection system in EMs, n.d.). It is crucial for fine-tuning the beam position to achieve optimal imaging conditions tilt (Deflector/double-deflection system in EMs, n.d.).

The samples prepared for TEM are placed in the stage with an airlock using a sample holder. Every electron microscope operates under a vacuum (e.g TEM JEM-1400 JEOL at 10^{-5} Pascal) that is achieved by a vacuum pump to avoid electron scattering due to gas molecules. Due to this vacuum, any hydrated biological sample analysed by TEM at room temperatures needs to be dehydrated. When working with biological samples, their contrast needs to be increased prior to analysis by TEM, due to their elemental composition being the same as the embedding resins used in sample preparation. This would lead to similar electron scattering and therefore low amplitude contrast. To increase contrast, salts of heavy metals are used, such as uranyl acetate or lead citrate. Furthermore, the sample should not be thicker than approximately 100 nm (depending on the used accelerating voltage), thus allowing the electrons to penetrate through the object.

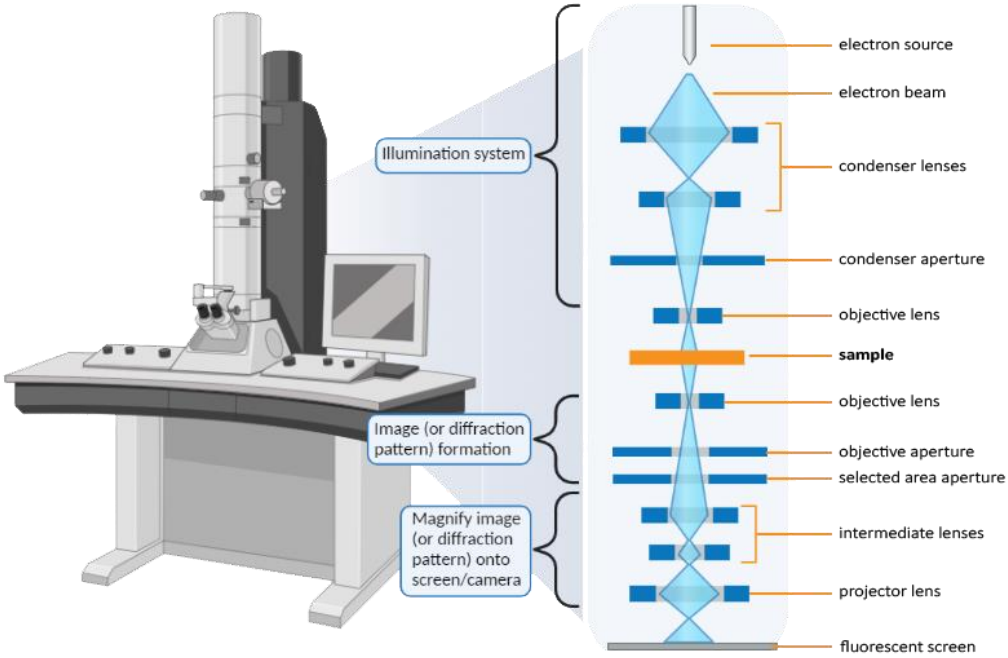

Figure 3: A simplified diagram of a transmission electron microscope highlighting the main parts (Transmission Electron Microscopy, n.d.).

2. Aim of the work

The aim of this bachelor work was to prepare biological specimens of lung tissue for transmission electron microscopy analysis. The prepared lung tissue samples, both the control and infected, were then analysed using the TEM JEM-1400 JEOL. The desired outcome was to observe and describe the ultrastructural changes associated with the replication of the SARS-CoV-2 virus, to better understand its impact on lung tissue and the consequences of SARS-CoV-2 virus infection.

3. Materials and Methods

3. 1. Samples

The research was performed on lung tissue from humanized mice, which had the human ACE2 receptor inserted. The mice were infected with the alpha variant of the SARS-CoV-2 virus. Both the control and infected mouse 2 and 5 days post infection lung specimens of humanized mice were provided by M. Palus, Ph.D. from the Laboratory of Arbovirology at the Institute of Parasitology, Biology centre.

3. 2. Chemicals

All chemicals used were in practical grade (p. A.) purity or electron microscopy (EM) grade. The used chemicals are presented in the following Table 1.

Name	Supplier
Glutaraldehyde (GA)	SPI
Formaldehyde	Polysciences
Sodium cacodylate	Polaron Equipment
Calcium Chloride ($CaCl_2$)	Sigma Aldrich
Sodium cacodylate with $CaCl_2$	Sigma Aldrich
Sodium cacodylate	Serva
Osmium Tetroxide (OsO_4)	SPI
Potassium hexacyanoferrate (II) trihydrate	Sigma Aldrich
Thiocarbonhydrazide	Sigma Aldrich
Uranyl acetate	EMS
Lead nitrate	Analar
L-aspartic acid	Serva
KOH	Sigma
Acetone	PELCO
Hard plus Resin 812	EMS

Table 1. Used chemicals in the preparation of samples.

3. 3. Sample preparation

Firstly, the lung tissues had to be fixed and stained. Dissected lungs were cut into small pieces and subsequently immersed in a solution of 2,5% Glutaraldehyde with 2% Formaldehyde (freshly made), with 2mM Calcium Chloride in a 0.15M cacodylate buffer with a pH of 7.4 at a temperature of 4 degrees Celsius overnight. To prepare the Formaldehyde solution, 2 grams of Paraformaldehyde were dissolved in 40 ml of water which was then heated to 65 degrees Celsius, and approximately 10-20 μl of 10N NaOH solution were added until the solution turned clear. The solution was then cooled to room temperature, and 50 ml of 0.3M Sodium Cacodylate with the 4mM $CaCl_2$ were added. The pH was checked to make sure that it is at 7.4. Finally, 10 ml of 25% Glutaraldehyde were added, and the fixative was stored at room temperature before it was used.

After fixation of the samples, they were rinsed 5 times, each for 3 minutes in a 150mM Sodium Cacodylate with 2mM $CaCl_2$. The samples were rinsed in glass bottles which were placed on a shaker. The volume of the Cacodylate buffer was 10 ml per one glass bottle.

Then the samples had to be post-fixed. The samples were post-fixed in 2% Osmium Tetroxide for 1.5 hours at room temperature, and then in 2.5% Potassium ferrocyanide, for the same amount of time at room temperature as well.

Next the samples were washed three times in the buffer, incubated with 1 % aqueous solution of Thiocarbohydrazide (TCH) for 2 hours, rinsed in double distilled water before being post-fixed in 2% Osmium Tetroxide for 4 hours at room temperature. After being washed in double distilled water again, the samples were immersed in 1% solution of aqueous Uranyl Acetate overnight at 4 degrees Celsius and washed again.

The washed samples were then put on a Walton Blok, where they were incubated in a Walton´s lead aspartate solution for 2 hours at 60 degrees Celsius. The Walton's solution consists of 0.998 grams of L-aspartic acid diluted in 250 ml of double distilled water, in order to prepare a 0.3 M stock solution.

Subsequently, 0.666 grams of Lead nitrate were dissolved in 10 ml of 0.03 M L-aspartic acid, and the pH of the solution was adjusted 1N KOH, to achieve the pH of 5.5. The samples were dehydrated using acetone in increasing concentrations, from 30-100%, for 15 minutes at each concentration.

The last step was the infiltration of the samples using resin. The infiltration of the samples was done using different concentrations of Hard Plus Resin 812 (EMS, 14115). It is done in steps and the resin is diluted with 100% acetone. Firstly with 25% Hard Plus Resin 812 in 100% acetone for 1 hour, then 50% Hard Plus Resin 812 in 100% acetone for one hour, then 75% Hard Plus Resin 812 in 100% acetone for one hour, and finally 100% Hard Plus Resin 812 overnight. The samples were then embedded using flat moulds and cured by polymerization for 48 hours at 60 degrees Celsius.

Before being analysed by the microscope, the samples were trimmed. Using a diamond knife, ultrathin sections (70 nm) were cut using an ultramicrotome and placed on TEM grids and carbon coated.

For the VERO samples, the sample preparation was similar to the lung tissue samples, the procedure differing in the usage of Ferrocyanide, Thiocarbohydrazide and subsequent osmification (Osmium Tetroxide was used only once). Uranyl acetate was not used, and neither was the Lead aspartate solution. The type of resin used EMBed 812 (EMS). The rest of the procedure for sample preparation was the same as described above.

In this work, various samples of lung tissue were analysed using the transmission electron microscope (Figure 4). From each tissue sample, pictures of the ultrastructure were obtained using the CMOS camera.

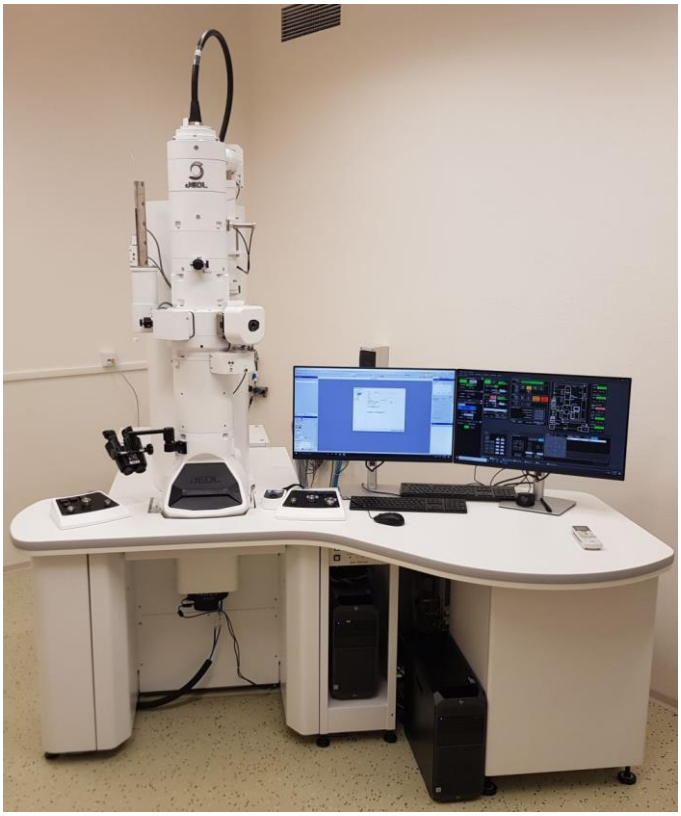

Figure 4: Transmission electron microscope TEM JEM-1400 JEOL, located at the Laboratory of Electron Microscopy in České Budějovice (BIOLOGICKÉ CENTRUM AV ČR, v. v. I. | Mikroskopy a Počítače pro Zpracování Dat, n.d.).

4. Results

The following images were taken as part of training (handling of the microscope and observing ultrastructural changes) with the VERO cell lineage. Figure 5 shows an image of a necrotic cell and Figure 6 shows several virion particles of the SARS-CoV-2 virus. Both images are from a sample 5 days post infection. In Figure 6, the characteristic round shape and the protruding spike glycoproteins S of the SARS-CoV-2 virion can be clearly observed.

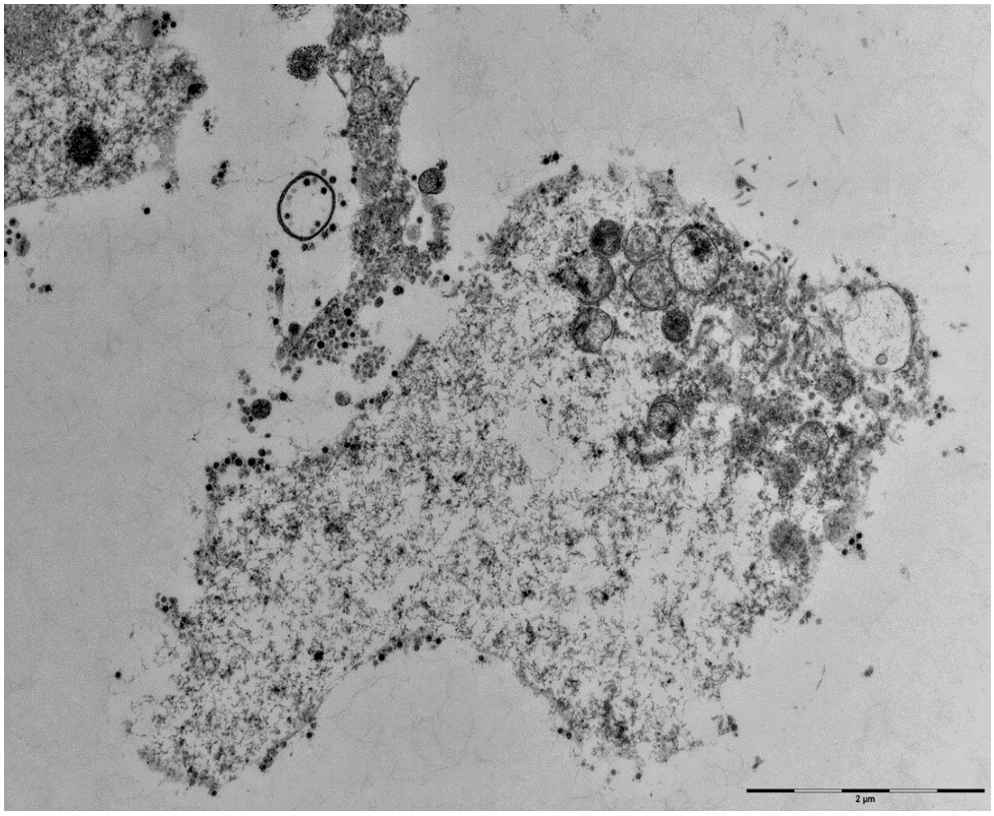

Figure 5: Necrotic cell found in the VERO cell lineage.

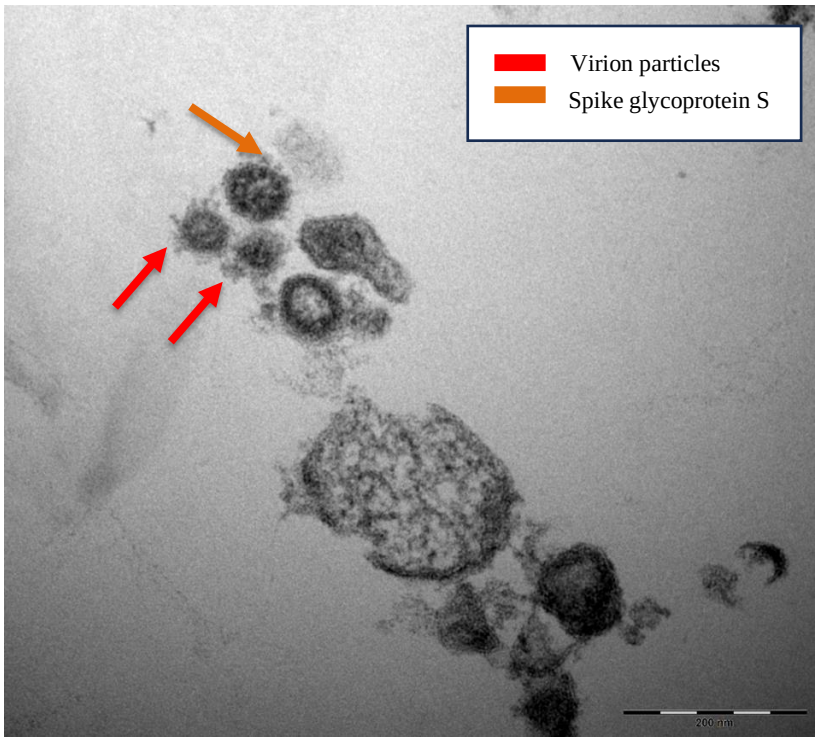

Figure 6: Virion particles of the SARS-CoV-2 virus found in the extracellular space. Red arrow indicates the virion particles, orange arrow the typical spike glycoproteins S on the surface of the virion.

Most of the following images are of the samples infected by the alpha variant, 2 days post infection. Viral replication sites were not found in the lung tissue, but ultrastructural changes related to a viral infection were observed.

The most prominent observed change was the presence of numerous immune cells in the infected tissues, specifically macrophages, which are a type of white blood cells. They were found in the alveolar space, usually in direct contact with pneumocytes (Figures 7,9), but also crossing from one acinus to another (Figure 8). They make contact with neighbouring cells using long extensions (pseudopods), which can be seen in Figures 7,8 and 9.

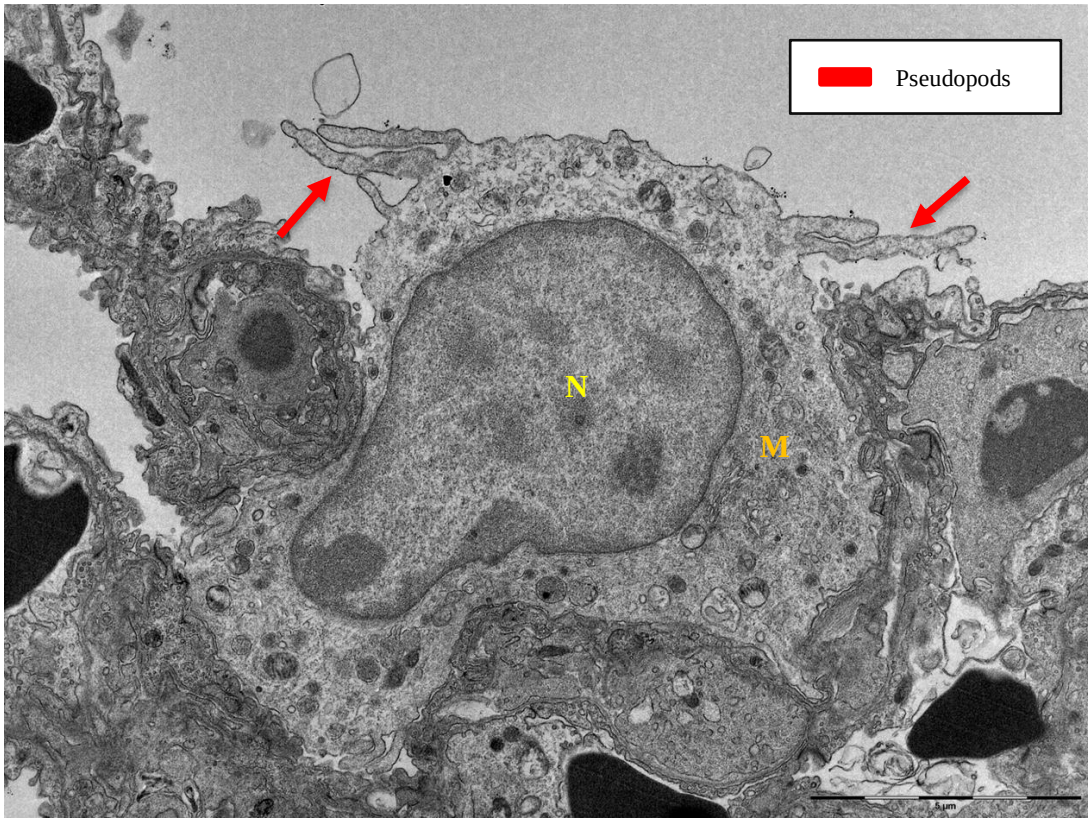

Figure 7: TEM micrograph of lung infected with alpha variant, 2 dpi. Macrophage in the alveolar space between alveolar cells. Macrophage (M), nucleus (N), red arrows point to pseudopods.

Figure 7 shows a macrophage between alveolar cells, and the long pseudopods can be very clearly seen extending above, around and between the adjoining cells. The macrophage has an irregular shape. The cells' structure is intact and there are no signs of a broken membrane or cell rupturing. The macrophage contains a large

nucleus, mitochondria and many lysosomes in various stages of development. Primary lysosomes are the smaller, darker vesicles containing lysosomal enzymes. The larger vesicles are secondary lysosomes. These organelles are best visible in Figure 10.

In Figure 8 another macrophage is depicted which was located passing through one acinus to another one. Structurally, it resembles the findings described in Figure 7. At the bottom of the macrophage, its curved and extending pseudopods can once again be observed. At the very right side of the image, a part of what could be described to be a necrotic cell and its remains can be found. Any further signs of ruptured or necrotic cells were not observed at this specific site.

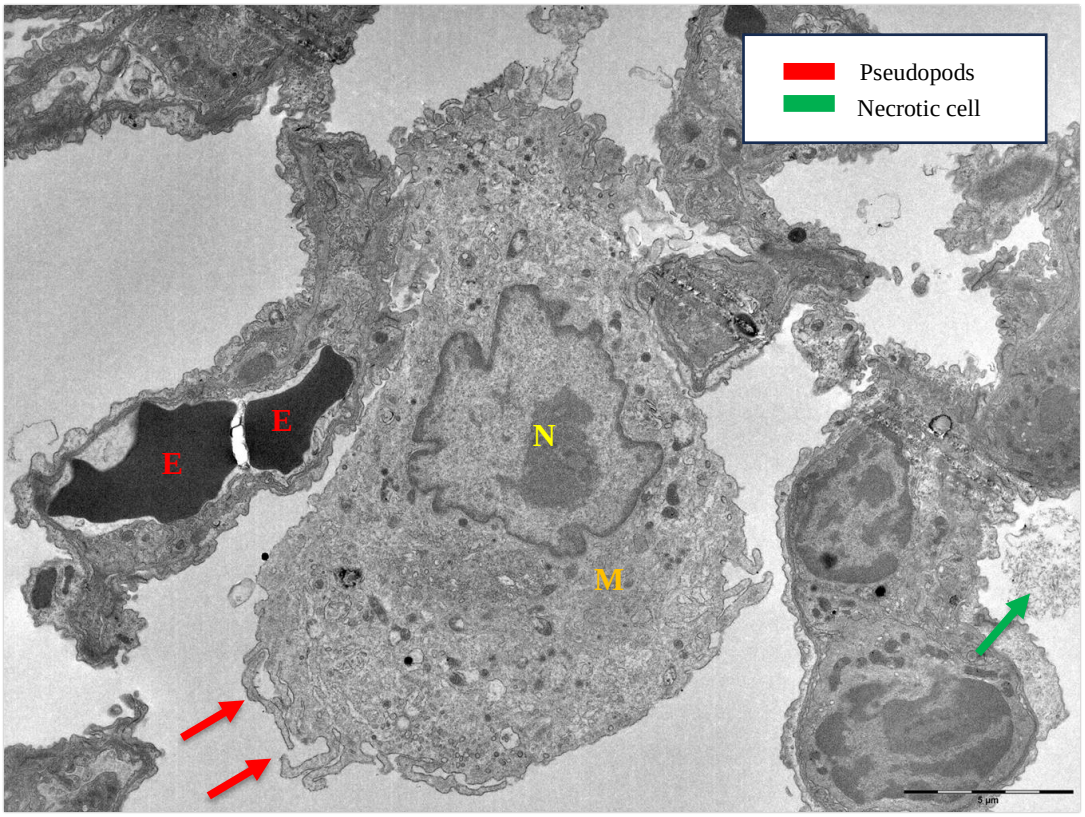

Figure 8: TEM micrograph of lung infected with alpha variant, 2 dpi. Macrophage (M) with a nucleus (N) and pseudopods (red arrows), passing through one acinus to another, erythrocytes (E) and a necrotic cell (green arrow).

More evidence of macrophages in the lung tissue is presented in Figure 9. The image shows a macrophage in very close proximity to necrotic cell debris in the airspace (red arrows in Figure 9).

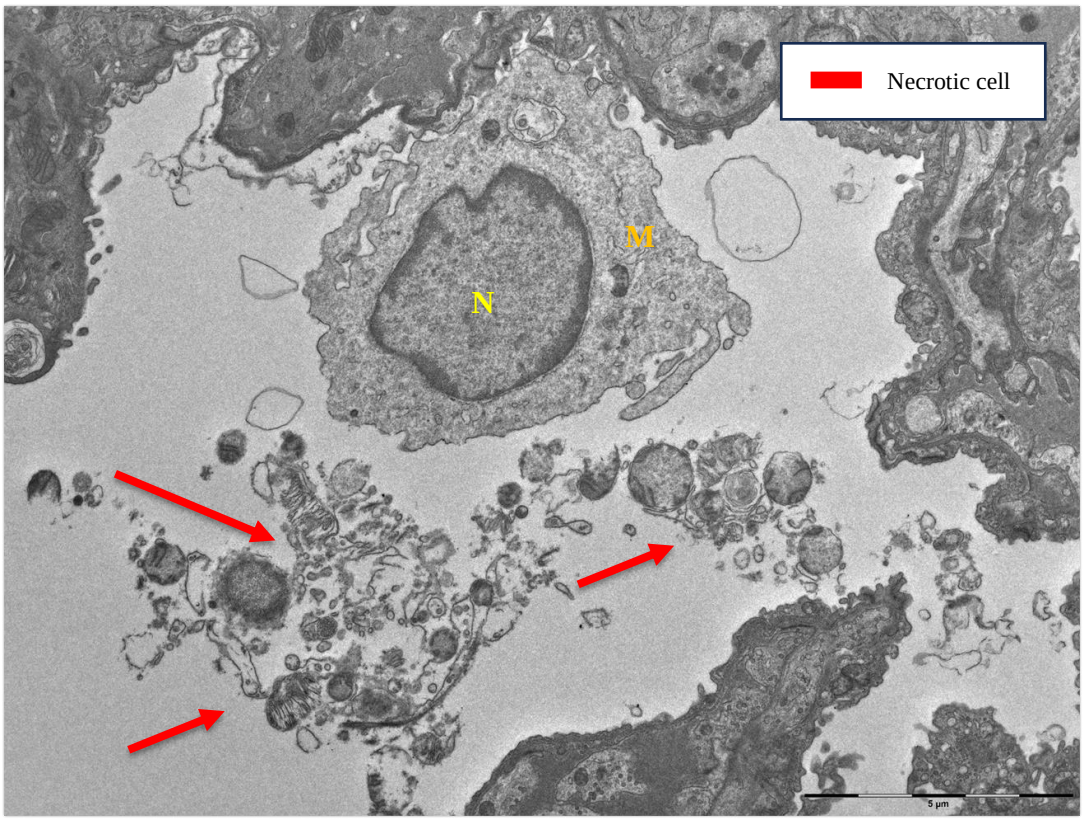

Figure 9: TEM micrograph of lung infected with alpha variant, 2 dpi. Necrotic cell is indicated by a red arrow.

More necrotic structures were observed, a necrotic mitochondrion (red arrows in Figure 10) was found very close to a pseudopod of a macrophage (orange arrows in Figure 10). There are three damaged mitochondria visible. The mitochondria on the far left has a ruptured double membrane that can be clearly seen, the other two mitochondria may have ruptured elsewhere. In the other two mitochondria the membranes are still partially preserved, but they are swollen and as the volume has increased, they have ruptured somewhere along their volume and the contents have spilled out.

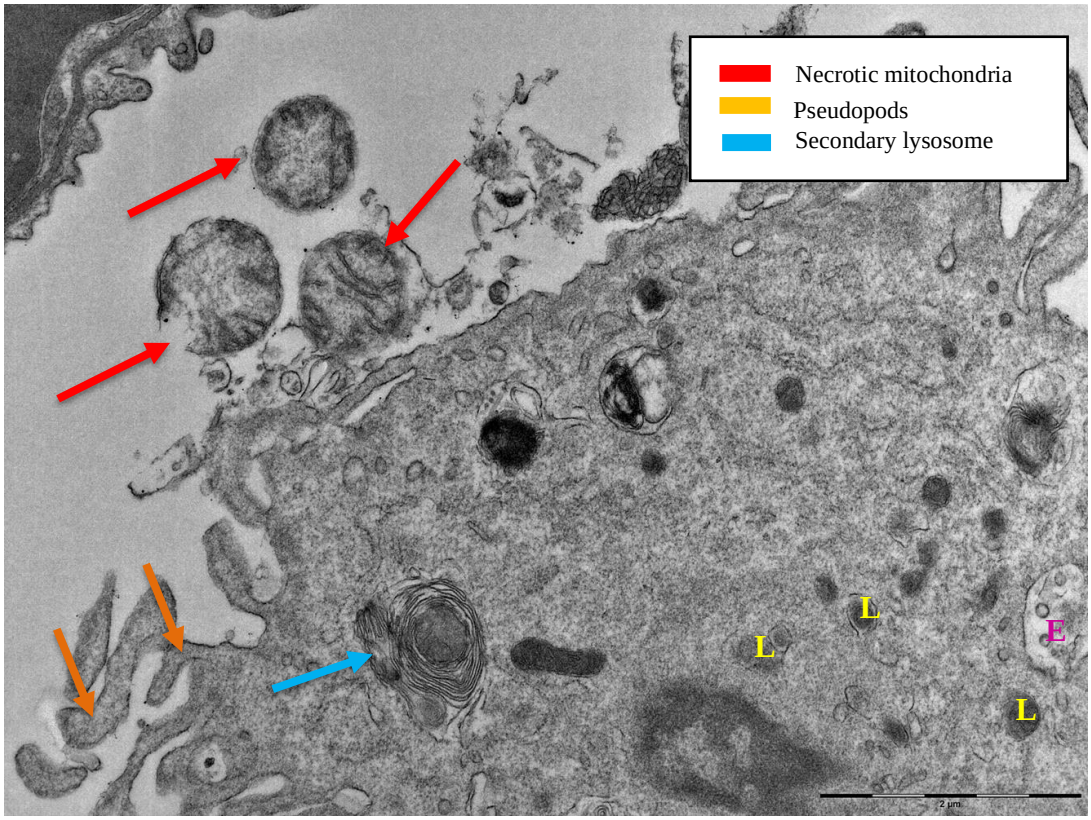

Figure 10: TEM micrograph of lung infected with alpha variant, 2 dpi. Necrotic mitochondria with ruptured membranes in close proximity to a macrophage and its pseudopods. Red arrow shows the necrotic mitochondria, the one on the left has a ruptured membrane. Orange arrows indicate the pseudopods of a macrophage. Blue arrows point to a secondary lysosome of the macrophage. The yellow "L" marks primary lysosomes. Pink "E" marks a late endosome.

Endothelial damage was also observed, as displayed in Figures 11 and 12. For comparison, Figure 11 shows a healthy endothelial cell, indicated by a green arrow, and a damaged endothelial cell (red arrow). The visible ultrastructural changes of the endothelium are swelling, change in shape which ties in with loss of membrane integrity. In the healthy endothelial cell in Figure 11 we can observe the nucleus, numerous small vesicles and mitochondria.

Swelling and damage of pneumocyte type 1 was also observed, with abnormal swollen mitochondria (Figure 11). In Figure 12, apart from endothelial damage, pneumocytes were also found to be affected by the apparent swelling of the cell content/ cytoplasm with a ruptured plasma membrane, followed by leakage of the

cell content into the alveolar space. Inside of the necrotic cytoplasm, lamellar structures were often present (yellow arrows in Figure 11).

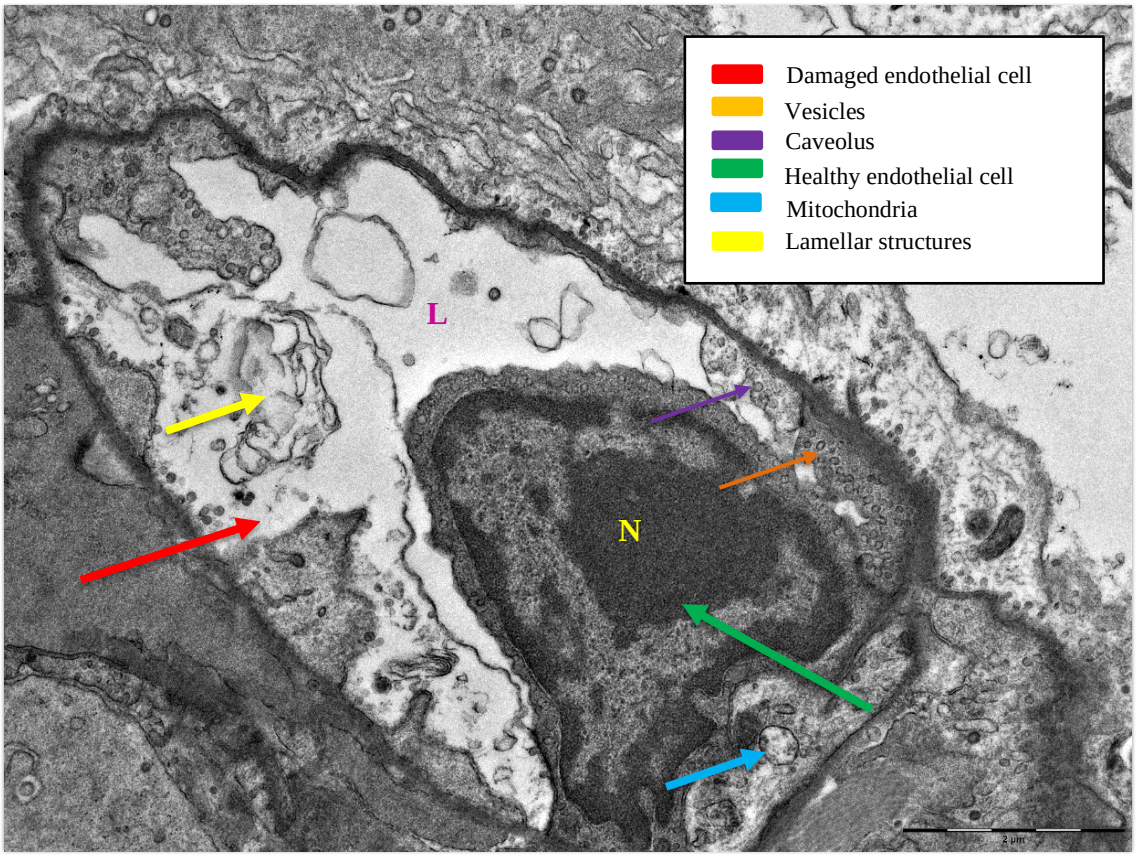

Figure 11: TEM micrograph of lung infected with alpha variant, 2 dpi. Red arrow indicates damaged endothelial cell, green arrow a healthy endothelial cell. Nucleus (N), lumen (L), caveolus (purple arrow), vesicles (orange arrow), mitochondria (blue arrow).

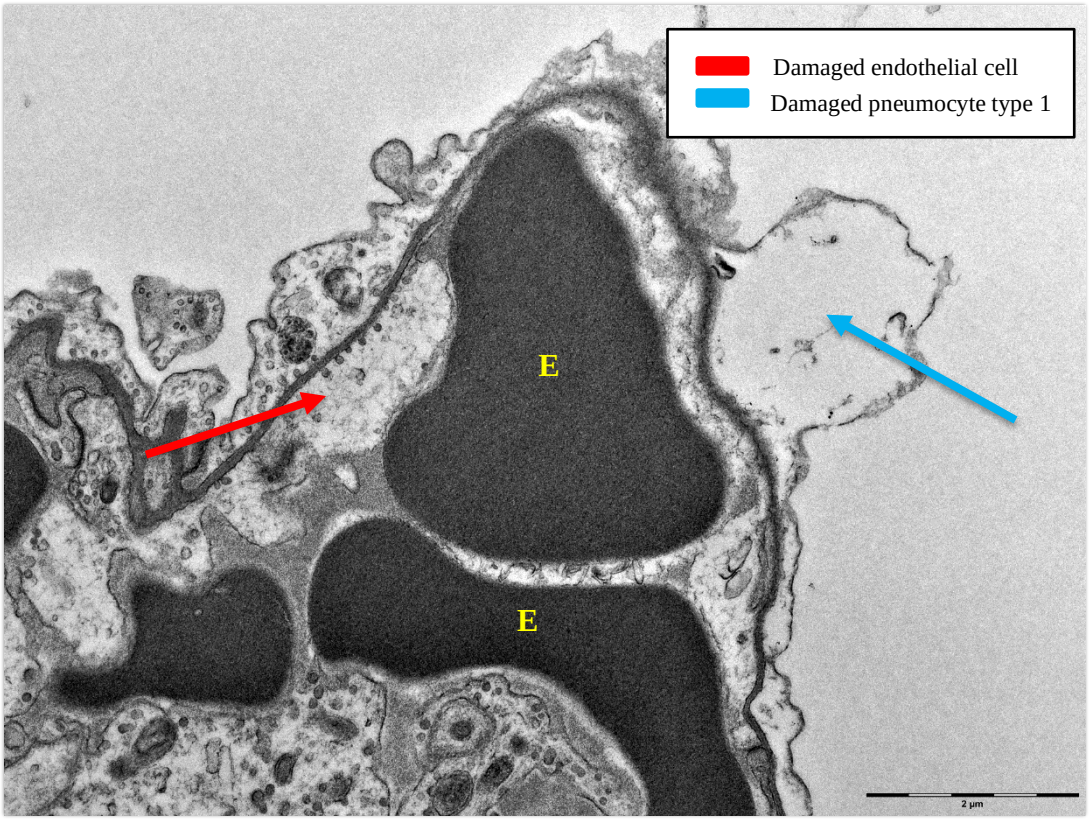

Figure 12: TEM micrograph of lung infected with alpha variant, 2 dpi. Damaged endothelial cell (red arrow), as well a damaged pneumocyte type 1 cell (blue arrow). Erythrocyte (E).

The transmission electron microscopy showed necrotic pneumocyte type 1 indicated by red arrows in Figure 13 and Figure 14, with a swollen appearance and disruption of the plasma membrane. For comparison, healthy pneumocytes of type 1 and 2 are shown in Figure 15.

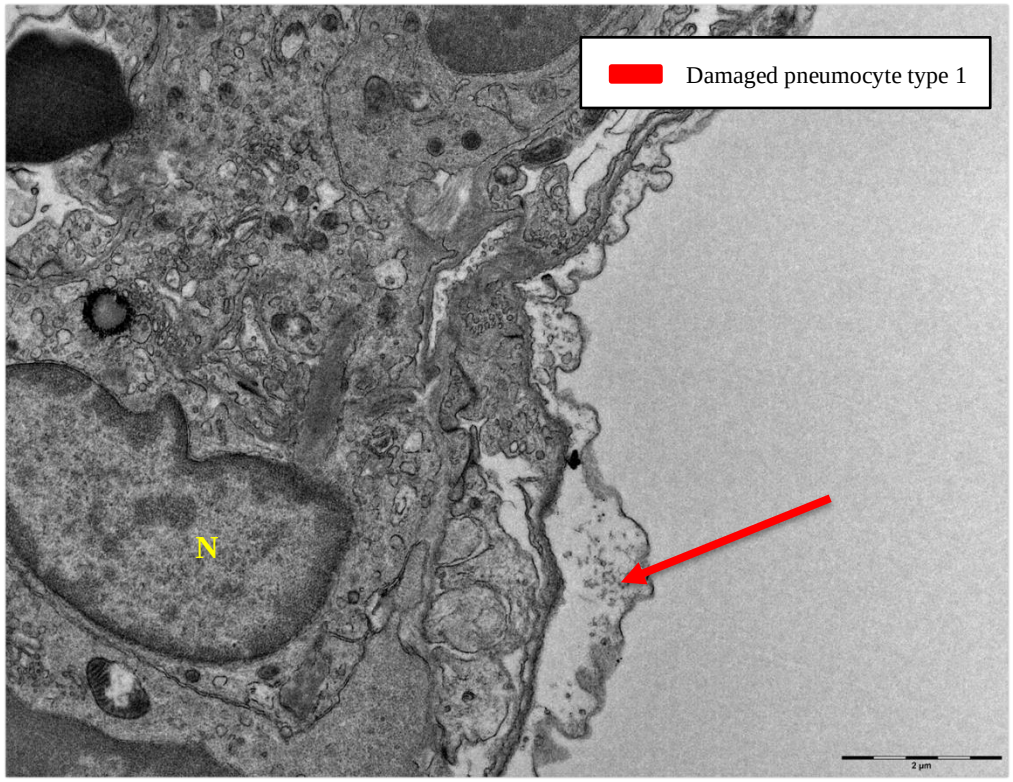

Figure 13: TEM micrograph of lung infected with alpha variant, 2 dpi. Damaged pneumocyte type 1 cell. Nucleus (N).

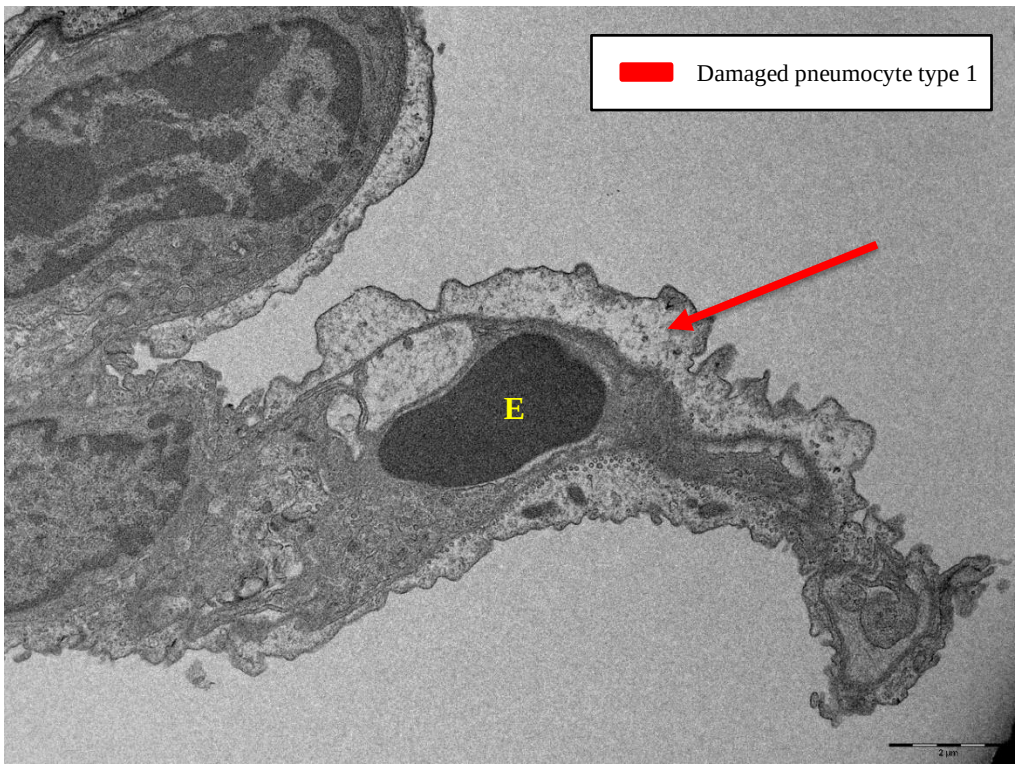

Figure 14: TEM micrograph of lung infected with alpha variant, 2 dpi. Damaged pneumocyte type 1 cell. Erythrocyte (E).

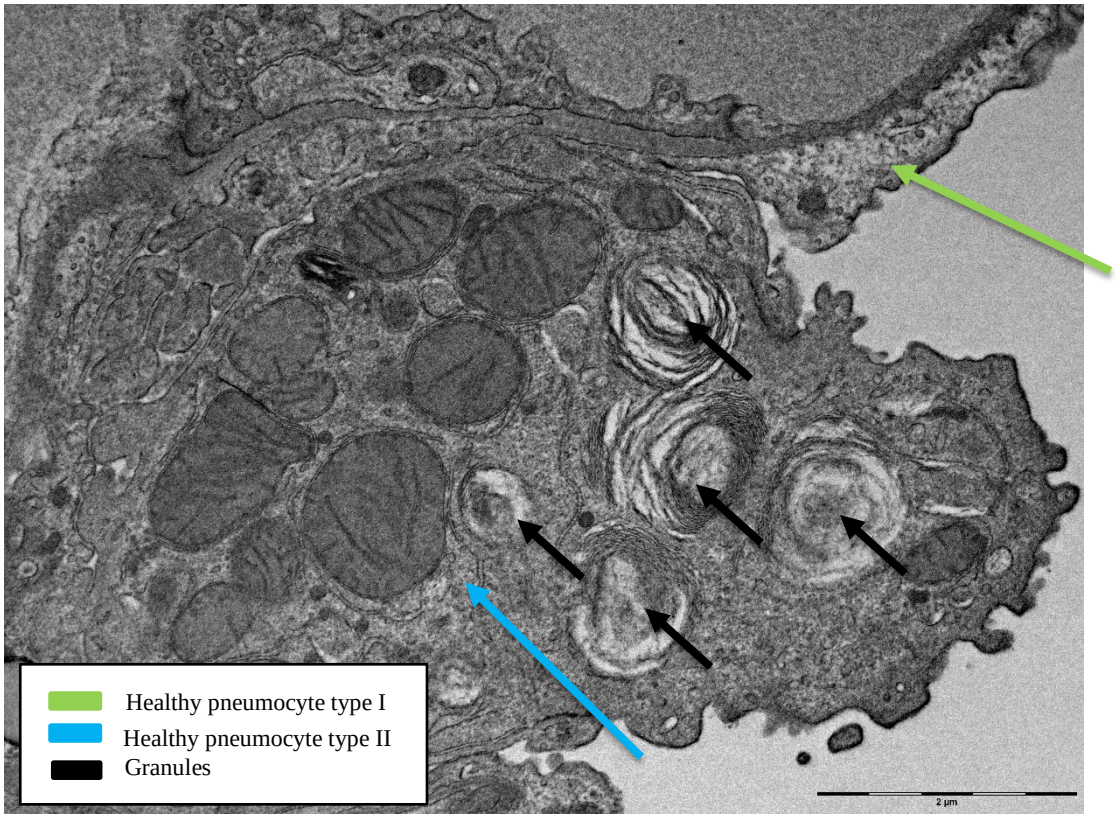

Figure 15: TEM micrograph of lung infected with alpha variant, 2 dpi. Healthy pneumocyte type 1 is indicated with a green arrow, pneumocyte type 2 with a blue arrow. Pneumocyte type 2 cells are able to synthesize alveolar surfactant, which is contained in granules. The black arrows point to the granules.

Damage near the pleura was observed (Figure 16), specifically there were damaged cells beneath the pleura. The necrotic area beneath the pleura contained necrotic cells. The necrotic area is indicated with a red arrow (Figure 16).

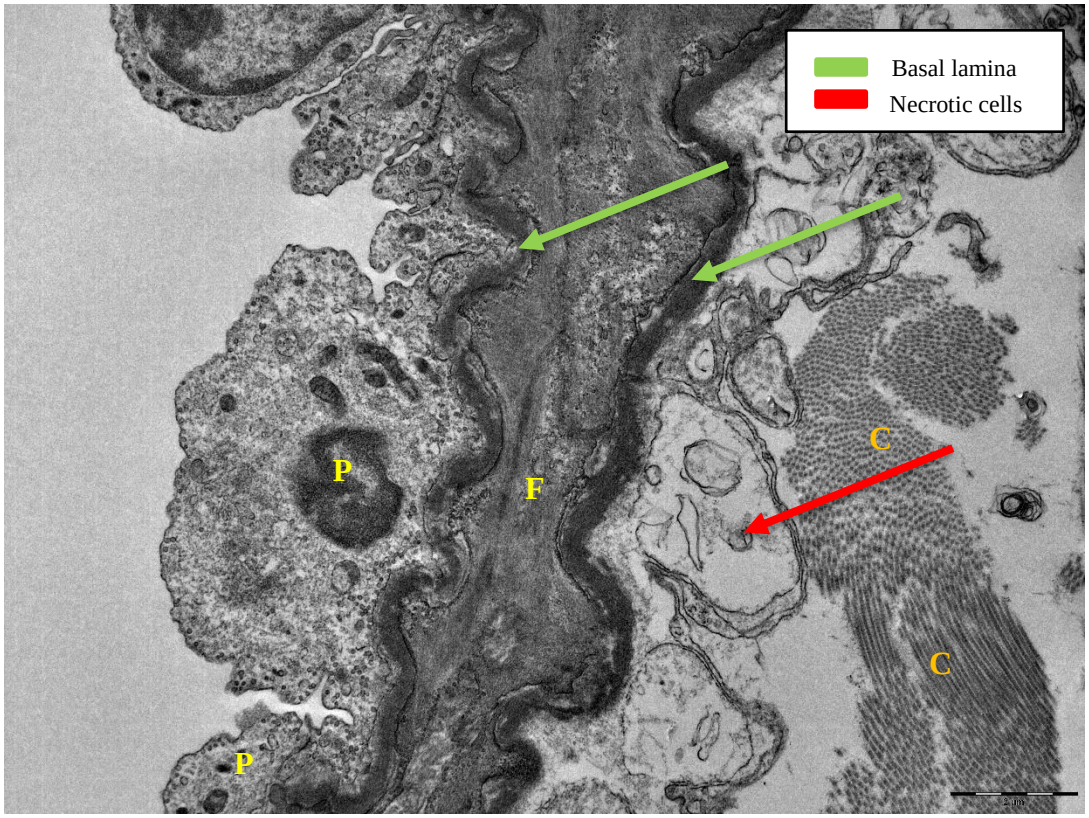

Figure 16: TEM micrograph of lung infected with alpha variant, 2 dpi. Pleura (P) with a necrotic area, necrotic cells (red arrow). Longitudinal sections of collagen fibers (C). Basal lamina (green arrows), fibroblasts (F).

5. Discussion

This work showed and analysed the ultrastructural changes present in lung tissues of humanized mice (modified with the ACE2 receptor) after infection with SARS-CoV-2 virus. The images presented in this thesis are mostly all of the sample infected with the alpha variant, 2 days post infection. It was expected that viral replication sites would be found in the cytoplasm, since single strand RNA viruses directly replicate at the ribosomes in the cytoplasm. A cytoplasmic replication complex should therefore be observable (reviewed by Hopfer et al., 2021). Assembled SARS-CoV-2 virions should be found within vacuoles, and in double membrane vesicles. Double membrane vesicles are the dominant structure of the cytoplasmic replication complex, as they are the initial site of viral replication (reviewed by Hopfer et al., 2021). They are of oval shape, and usually found in clusters of 200 nm (reviewed by Hopfer et al., 2021). These arrangements would

be expected predominantly in the samples 2 days post infection. However, viral replication sites were not observed in any analysed samples. Nonetheless, the viral replication sites (data not shown) and virion particles were observed in the VERO cells, as presented in Section 4, Figures 5 and 6.

A major observation of this study was the large number of ultrastructural changes found in the samples 2 dpi infected by the alpha variant. The aim was to describe ultrastructural changes in cells infected by the virus in vivo, and the most dominant changes observed in the lung tissues were the abundant presence of macrophages in the alveolar space, cell damage of the epithelium and of pneumocytes type 1, and necrosis of cells.

The large number of macrophages present in the observed samples confirms information from other studies, which stated that the presence of inflammatory cells and their infiltration is among the initial pathological signs observed in SARS-CoV-2 infections in human autopsies (reviewed by Bridges et al., 2022; Martines et al., 2020; Tian et al., 2020), and in humanized mouse models (Winkler et al., 2020). An increased number of macrophages was also observed also in a study by Delorey et al. (2021) and a study done by Valdebenito et al. (2021), where they studied the human lung (Delorey et al., 2021; Valdebenito et al., 2021).

Macrophages can be classified into two different phenotypes; the conventionally activated phenotype M1 and the alternatively activated phenotype M2, depending on the local environmental variables that stimulate them (reviewed by Cheng et al., 2021; Mills et al., 2000; reviewed by Puttur et al., 2019; reviewed by Sica & Mantovani, 2012). According to data, M1 is strongly associated with pro-inflammatory responses, whereas M2 is crucial for anti-inflammatory responses (Sica & Mantovani, 2012). M2 macrophages may be further classified based on stimulators triggering their activation (reviewed by Cheng et al., 2021; Mills et al., 2000; reviewed by Puttur et al., 2019; reviewed by Sica & Mantovani, 2012). While M2 macrophages are primarily linked to the resolution phase of inflammation during acute lung injury, M1 phenotypes of macrophages are engaged in the acute phase (Johnston et al., 2012).

The observed macrophages were activated based on the observed presence of numerous lysosomes and phagolysosomes (Figure 10), which declares their increased phagocytic activity (Melo & Dvorak, 2012; reviewed in Melo et al., 2011).

Another sign of activation is the presence of lipid droplets in the macrophage cytoplasm. According to a 2011 study (Melo et al., 2011), immune system cells, especially macrophages, eosinophils, and neutrophils, quickly produce lipid bodies in response to various inflammatory disorders. These lipid bodies act as intracellular sites for the synthesis of inflammatory lipid mediators (Melo et al., 2011). Typically, macrophages have few cytoplasmic lipid bodies, but when they get into contact with pathogens like bacteria and parasites or inflammatory stimuli, they can be quickly stimulated to produce additional lipid bodies (D'Avila et al., 2012; Melo & Dvorak, 2012; Melo et al., 2011; Saka & Valdivia, 2012).

The formation of pseudopodia (Figures 7-10), which are finger-like extensions of the plasma membrane, was also observed. One of the categories of pseudopodia are called filopodia (Dustin et al., 2018). In general, pseudopodia are broader, more irregular extensions involved in amoeboid movement and phagocytosis, while filopodia tend to be thinner, more elongated extensions that primarily serve as guidance structures for directed cell migration and environmental sensing (Dustin et al., 2018). In Figures 8 and 10, the extensions with which macrophages make contact with neighbouring cells and the targeted pathogens appear to resemble those of filopodia more closely.

A predominantly euchromatic nucleus is a characteristic of activated macrophages that is in accordance with other studies (Dias et al., 2011; Melo et al., 2003; Melo et al., 2006). They stated that ultrastructure of macrophages containing newly formed lipid bodies in response to inflammatory diseases has some typical morphological characteristics, for instance a higher amount of vesicles and projections on the cell surface, a prominent Golgi complex or a nucleus that is mostly euchromatic. These are all markers of cell activation.

Apart from macrophages, large amounts of necrotic cells and necrotic cell debris in the cellular space was observed. This suggests cell death, which may have been caused by either viral replication or subsequent inflammatory response (Channappanavar et al., 2016).

The ACE2 receptor is expressed in many cells in the body, including pneumocytes of type 1 and 2 and alveolar epithelial cells. Because of this, it can be expected that ultrastructural changes will most likely occur in these cells. A study from 2020 stated that since SARS-CoV-2 is able to enter type 1 and type 2 pneumocytes and the endothelium, a diffuse inflammatory effect is expected in these cells which can cause cellular lysis (Oliveira et al., 2020). Lysis was observed in our samples as well. The inflammatory cascade in the cells leads to an increased production of interleukins and damage to epithelium and endothelium. These changes were observed in our samples, but without any presence of viral particles. It can therefore be assumed that the necrosis was caused by an inflammatory cascade (Oliveira et al., 2020). A possible explanation for these ultrastructural changes occurring mainly in pneumocytes in samples only 2 days post infection, is provided in a study from 2004 (Hamming et al., 2004). It states that alveolar pneumocytes are a possible entrance point for SARS-CoV-2. This rapid progression could be the cause of the severe alveolar damage observed in samples 2 days post infection.

6. Conclusion

In conclusion, this work described and analysed ultrastructural changes in humanized murine lungs upon infection with the alpha variant of SARS-CoV-2 using transmission electron microscopy. It was concluded that since no viruses or viral replication sites were observed in the tissues, it can be assumed that their damage was not caused by direct infection of SARS-CoV-2, but most likely by the inflammatory response that followed it (reviewed by Bridges et al., 2022; Y. J. Hou et al., 2020; Martines et al., 2020). The observed changes on the ultrastructural level involve irreversible damage leading to necrosis of endothelial cells and of pneumocytes type 1 cells, which were accompanied by the presence of macrophages.

7. References

Ammerman, N. C., Beier-Sexton, M., & Azad, A. F. (2008). Growth and Maintenance of Vero Cell Lines. Current Protocols in Microbiology. https://doi.org/10.1002/9780471729259.mca04es11

BIOLOGICKÉ CENTRUM AV ČR, v. v. i. | Mikroskopy a počítače pro zpracování dat. (n.d.). Www.bc.cas.cz. https://www.bc.cas.cz/servisni-pracoviste/laborator-elektronove-mikroskopie/informace-pro-uzivatele/mikroskopy/#anchor

Bridges, J. P., Vladar, E. K., Huang, H., & Mason, R. J. (2022). Respiratory epithelial cell responses to SARS-CoV-2 in COVID-19. Thorax, 77(2), 203–209. https://doi.org/10.1136/thoraxjnl-2021-217561

C. Barry Carter, & Williams, D. B. (1996). Transmission Electron Microscopy. In Springer eBooks. https://doi.org/10.1007/978-1-4757-2519-3

Centers for Disease Control and Prevention. (2022, August 16). CDC Museum COVID-19 Timeline. Centers for Disease Control and Prevention; CDC. https://www.cdc.gov/museum/timeline/covid19.html

Channappanavar, R., Fehr, A. R., Vijay, R., Mack, M., Zhao, J., Meyerholz, D. K., & Perlman, S. (2016). Dysregulated Type I Interferon and Inflammatory Monocyte-Macrophage Responses Cause Lethal Pneumonia in SARS-CoV-Infected Mice. Cell Host & Microbe, 19(2), 181–193. https://doi.org/10.1016/j.chom.2016.01.007

Chaudhry R, Bordoni B. Anatomy, Thorax, Lungs. [Updated 2022 Jul 25]. In: StatPearls [Internet]. Treasure Island (FL): StatPearls Publishing; 2023 Jan-. Available from: https://www.ncbi.nlm.nih.gov/books/NBK470197/

Cheng, P., Li, S., & Chen, H. (2021). Macrophages in Lung Injury, Repair, and Fibrosis. Cells, 10(2), 436. https://doi.org/10.3390/cells10020436

D'Avila, H., Toledo, D. A. M., & Melo, R. C. N. (2012). Lipid Bodies: Inflammatory Organelles Implicated in Host-Trypanosoma cruziInterplay during Innate Immune Responses. Mediators of Inflammation, 2012, 1–11. https://doi.org/10.1155/2012/478601

Delorey, T. M., Ziegler, C. G. K., Heimberg, G., Normand, R., Yang, Y., Segerstolpe, Å., Abbondanza, D., Fleming, S. J., Subramanian, A., Montoro, D. T., Jagadeesh, K. A., Dey, K. K., Sen, P., Slyper, M., Pita-Juárez, Y. H., Phillips, D., Biermann, J., Bloom- Ackermann, Z., Barkas, N., … Regev, A. (2021). COVID-19 tissue atlases reveal SARS-CoV-2 pathology and cellular targets. Nature, 595(7865), Article 7865. https://doi.org/10.1038/s41586-021-03570-8

Deflector/double-deflection system in EMs. (n.d.). Www.globalsino.com. https://www.globalsino.com/EM/page3764.html

Dias, F. F., Chiarini-Garcia, H., Parreira, G. G., & Melo, R. C. N. (2011). Mice Spermatogonial Stem Cells Transplantation Induces Macrophage Migration into the Seminiferous Epithelium and Lipid Body Formation: High-Resolution Light Microscopy and Ultrastructural Studies. Microscopy and Microanalysis, 17(6), 1002–1014. https://doi.org/10.1017/s1431927611012098

Dustin M.E. Lillico, Pemberton, J., & Stafford, J. L. (2018). Selective Regulation of Cytoskeletal Dynamics and Filopodia Formation by Teleost Leukocyte Immune-Type Receptors Differentially Contributes to Target Capture During the Phagocytic Process. Frontiers in Immunology, 9. https://doi.org/10.3389/fimmu.2018.01144

Electron Microscopy. (2014). In J. Kuo (Ed.), Methods in Molecular Biology. Humana Press. https://doi.org/10.1007/978-1-62703-776-1

Fehr, A. R., & Perlman, S. (2015). Coronaviruses: An Overview of Their Replication and Pathogenesis. Coronaviruses, 1282, 1–23. https://doi.org/10.1007/978-1-4939-2438-7_1

Franken, L. E., Grünewald, K., Boekema, E. J., & Stuart, M. C. A. (2020). A Technical Introduction to Transmission Electron Microscopy for Soft-Matter: Imaging, Possibilities, Choices, and Technical Developments. Small, 16(14), 1906198. https://doi.org/10.1002/smll.201906198

Gartner, Leslie P., Stephen A. Morse. (1997). Color Textbook of Histology (-). Philadelphia: Philadelphia: Saunders Elsevier,.

Gillim-Ross, L., Taylor, J., Scholl, D. R., Ridenour, J., Masters, P. S., & Wentworth, D. E. (2004). Discovery of Novel Human and Animal Cells Infected by the Severe Acute Respiratory Syndrome Coronavirus by Replication-Specific Multiplex Reverse Transcription-PCR. Journal of Clinical Microbiology, 42(7), 3196–3206. https://doi.org/10.1128/jcm.42.7.3196-3206.2004

Goldsmith, C. S., Tatti, K. M., Ksiazek, T. G., Rollin, P. E., Comer, J. A., Lee, W. W., Rota, P. A., Bankamp, B., Bellini, W. J., & Zaki, S. R. (2004). Ultrastructural Characterization of SARS Coronavirus. Emerging Infectious Diseases, 10(2), 320–326. https://doi.org/10.3201/eid1002.030913

Gui, M., Song, W., Zhou, H., Xu, J., Chen, S., Xiang, Y., & Wang, X. (2016). Cryo-electron microscopy structures of the SARS-CoV spike glycoprotein reveal a

prerequisite conformational state for receptor binding. Cell Research, 27(1), 119–129. https://doi.org/10.1038/cr.2016.152

Hamming, I., Timens, W., Bulthuis, M., Lely, A., Navis, G., & van Goor, H. (2004). Tissue distribution of ACE2 protein, the functional receptor for SARS coronavirus. A first step in understanding SARS pathogenesis. The Journal of Pathology, 203(2), 631–637. https://doi.org/10.1002/path.1570

Harrison, A. G., Lin, T., & Wang, P. (2020). Mechanisms of SARS-CoV-2 Transmission and Pathogenesis. Trends in Immunology, 41(12), 1100–1115. https://doi.org/10.1016/j.it.2020.10.004

Hoffmann, M., Kleine-Weber, H., Schroeder, S., Krüger, N., Herrler, T., Erichsen, S., Schiergens, T. S., Herrler, G., Wu, N.-H., Nitsche, A., Müller, M. A., Drosten, C., & Pöhlmann, S. (2020). SARS-CoV-2 Cell Entry Depends on ACE2 and TMPRSS2 and Is Blocked by a Clinically Proven Protease Inhibitor. Cell, 181(2), 271–280. https://doi.org/10.1016/j.cell.2020.02.052

Hopfer, H., Herzig, M. C., Gosert, R., Menter, T., Hench, J., Tzankov, A., Hirsch, H. H., & Miller, S. E. (2021). Hunting coronavirus by transmission electron microscopy - a guide to SARS-CoV-2-associated ultrastructural pathology in COVID-19 tissues. Histopathology, 78(3), 358–370. https://doi.org/10.1111/his.14264

Hou, Y. J., Okuda, K., Edwards, C. E., Martinez, D. R., Asakura, T., Dinnon, K. H., Kato, T., Lee, R. E., Yount, B. L., Mascenik, T. M., Chen, G., Olivier, K. N., Ghio, A., Tse, L.V., Leist, S. R., Gralinski, L. E., Schäfer, A., Dang, H., Gilmore, R., … Baric, R. S. (2020). SARS-CoV-2 Reverse Genetics Reveals a Variable Infection Gradient in the Respiratory Tract. Cell, 182(2),429-446.e14. https://doi.org/10.1016/j.cell.2020.05.042

Hsia, C., Hyde, D., & Weibel, E. (2016). Lung Structure and the Intrinsic Challenges of Gas Exchange. Comprehensive Physiology, 6, 827–895. https://doi.org/10.1002/cphy.c150028

Jackson, C. B., Farzan, M., Chen, B., & Choe, H. (2022). Mechanisms of SARS-CoV-2 entry into cells. Nature Reviews Molecular Cell Biology, 23(1), Article 1. https://doi.org/10.1038/s41580-021-00418-x

Johnston, L. K., Rims, C. R., Gill, S. E., McGuire, J. K., & Manicone, A. M. (2012). Pulmonary Macrophage Subpopulations in the Induction and Resolution of Acute Lung Injury. American Journal of Respiratory Cell and Molecular Biology, 47(4), 417–426. https://doi.org/10.1165/rcmb.2012-0090oc

Kirchdoerfer, R. N., Cottrell, C. A., Wang, N., Pallesen, J., Yassine, H. M., Turner, H. L., Corbett, K. S., Graham, B. S., McLellan, J. S., & Ward, A. B. (2016). Pre-fusion structure of a human coronavirus spike protein. Nature, 531(7592), 118–121. https://doi.org/10.1038/nature17200

Knudsen, L., & Ochs, M. (2018). The micromechanics of lung alveoli: Structure and function of surfactant and tissue components. Histochemistry and Cell Biology, 150(6), 661– 676. https://doi.org/10.1007/s00418-018-1747-9

Lai C. C., Shih T. P., Ko W. C., Tang H. J., Hsueh P. R. (2020). Severe acute respiratory syndrome coronavirus 2 (SARS-CoV-2) and coronavirus disease-2019 (COVID-19): The epidemic and the challenges. Int. J. Antimicrobial Agents 55, 105924. doi: 10.1016/j.ijantimicag.2020.105924

Lu, R., Zhao, X., Li, J., Niu, P., Yang, B., Wu, H., Wang, W., Song, H., Huang, B., Zhu, N., Bi, Y., Ma, X., Zhan, F., Wang, L., Hu, T., Zhou, H., Hu, Z., Zhou, W., Zhao,

L., & Chen, J. (2020). Genomic characterisation and epidemiology of 2019 novel coronavirus: implications for virus origins and receptor binding. The Lancet, 395(10224). https://doi.org/10.1016/s0140-6736(20)30251-8

Mahabadi, N., Goizueta, A. A., & Bordoni, B. (2022). Anatomy, Thorax, Lung Pleura And Mediastinum. In StatPearls. StatPearls Publishing

Martines, R. B., Ritter, J. M., Matkovic, E., Gary, J., Bollweg, B. C., Bullock, H., Goldsmith,C. S., Silva-Flannery, L., Seixas, J. N., Reagan-Steiner, S., Uyeki, T., Denison, A., Bhatnagar, J., Shieh, W.-J., Zaki, S. R., & COVID-19 Pathology Working Group. (2020). Pathology and Pathogenesis of SARS-CoV-2 Associated with Fatal Coronavirus Disease, United States. Emerging Infectious Diseases, 26(9), 2005–2015. https://doi.org/10.3201/eid2609.202095

Melo, R. C., & Dvorak, A. M. (2012). Lipid body-phagosome interaction in macrophages during infectious diseases: host defense or pathogen survival strategy?. PLoS pathogens, 8(7), e1002729. https://doi.org/10.1371/journal.ppat.1002729

Melo, R. C., D'Avila, H., Fabrino, D. L., Almeida, P. E., & Bozza, P. T. (2003). Macrophage lipid body induction by Chagas disease in vivo: putative intracellular domains for eicosanoid formation during infection. Tissue & cell, 35(1), 59–67. https://doi.org/10.1016/s0040-8166(02)00105-2

Melo, R. C., D'Avila, H., Wan, H. C., Bozza, P. T., Dvorak, A. M., & Weller, P. F. (2011). Lipid bodies in inflammatory cells: structure, function, and current imaging techniques. The journal of histochemistry and cytochemistry : official journal of the Histochemistry Society, 59(5), 540–556. https://doi.org/10.1369/0022155411404073

Melo, R. C., Fabrino, D. L., Dias, F. F., & Parreira, G. G. (2006). Lipid bodies: Structural markers of inflammatory macrophages in innate immunity. Inflammation research : official journal of the European Histamine Research Society ... [et al.], 55(8), 342–348. https://doi.org/10.1007/s00011-006-5205-0

Mills, C. D., Kincaid, K., Alt, J. M., Heilman, M. J., & Hill, A. M. (2000). M-1/M-2 macrophages and the Th1/Th2 paradigm. Journal of Immunology (Baltimore, Md.: 1950), 164(12), 6166–6173. https://doi.org/10.4049/jimmunol.164.12.6166

Murgolo, N., Therien, A. G., Howell, B., Klein, D., Koeplinger, K., Lieberman, L. A., et al. (2021). SARS-CoV-2 tropism, entry, replication, and propagation: Considerations for drug discovery and development. PloS Pathog. 17, 1–18. https://www.frontiersin.org/articles/10.3389/fcimb.2022.1003608/full

Ochs, M., Hegermann, J., Lopez-Rodriguez, E., Timm, S., Nouailles, G., Matuszak, J.,Simmons, S., Witzenrath, M., & Kuebler, W. M. (2020). On Top of the Alveolar Epithelium: Surfactant and the Glycocalyx. International Journal of Molecular Sciences, 21(9), E3075. https://doi.org/10.3390/ijms21093075

Oliveira, T. L., Melo, I. S., Cardoso-Sousa, L., Santos, I. A., El Zoghbi, M. B., Shimoura, C. G., Georjutti, R. P., Castro, O. W., Goulart, L. R., Jardim, A. C. G., Cunha, T. M., & Sabino-Silva, R. (2020). Pathophysiology of SARS-CoV-2 in Lung of Diabetic Patients. Frontiers in Physiology, 11. https://doi.org/10.3389/fphys.2020.587013

Osada, N., Kohara, A., Yamaji, T., Hirayama, N., Kasai, F., Sekizuka, T., Kuroda, M., & Hanada, K. (2014). The Genome Landscape of the African Green Monkey Kidney-Derived Vero Cell Line. DNA Research, 21(6), 673–683. https://doi.org/10.1093/dnares/dsu029

Pallesen, J., Wang, N., Corbett, K. S., Wrapp, D., Kirchdoerfer, R. N., Turner, H. L., Cottrell, C. A., Becker, M. M., Wang, L., Shi, W., Kong, W.-P., Andres, E. L., Kettenbach, A. N., Denison, M. R., Chappell, J. D., Graham, B. S., Ward, A. B., & McLellan, J. S. (2017). Immunogenicity and structures of a rationally designed prefusion MERS-CoV spike antigen. Proceedings of the National Academy of Sciences, 114(35), E7348–E7357. https://doi.org/10.1073/pnas.1707304114

Perlman, S., & Netland, J. (2009). Coronaviruses post-SARS: Update on replication and pathogenesis. Nature Reviews. Microbiology, 7(6), 439–450. https://doi.org/10.1038/nrmicro2147

Pires De Souza, G. A., Le Bideau, M., Boschi, C., Wurtz, N., Colson, P., Aherfi, S., Devaux, C., & La Scola, B. (2022). Choosing a cellular model to study SARS-CoV-2. Frontiers in Cellular and Infection Microbiology, 12. https://doi.org/10.3389/fcimb.2022.1003608

Pizzato, M., Baraldi, C., Boscato Sopetto, G., Finozzi, D., Gentile, C., Gentile, M. D., Marconi, R., Paladino, D., Raoss, A., Riedmiller, I., Ur Rehman, H., Santini, A., Succetti, V., & Volpini, L. (2022). SARS-CoV-2 and the Host Cell: A Tale of Interactions. Frontiers in Virology, 1. https://doi.org/10.3389/fviro.2021.815388

Puttur, F., Gregory, L. G., & Lloyd, C. M. (2019). Airway macrophages as the guardians of tissue repair in the lung. Immunology & Cell Biology, 97(3), 246–257. https://doi.org/10.1111/imcb.12235

Ruaro, B., Salton, F., Braga, L., Wade, B., Confalonieri, P., Volpe, M. C., Baratella, E., Maiocchi, S., & Confalonieri, M. (2021). The History and Mystery of Alveolar Epithelial Type II Cells: Focus on Their Physiologic and Pathologic Role in

Lung. International Journal of Molecular Sciences, 22(5), Article 5. https://doi.org/10.3390/ijms22052566

Saka, H. A., & Valdivia, R. (2012). Emerging Roles for Lipid Droplets in Immunity and Host-Pathogen Interactions. Annual Review of Cell and Developmental Biology, 28(1), 411–437. https://doi.org/10.1146/annurev-cellbio-092910-153958

Sica, A., & Mantovani, A. (2012). Macrophage plasticity and polarization: in vivo veritas. Journal of Clinical Investigation, 122(3), 787–795. https://doi.org/10.1172/jci59643

Siu, Y. L., Teoh, K. T., Lo, J., Chan, C. M., Kien, F., Escriou, N., Tsao, S. W., Nicholls, J. M., Altmeyer, R., Peiris, J. S. M., Bruzzone, R., & Nal, B. (2008). The M, E, and N Structural Proteins of the Severe Acute Respiratory Syndrome Coronavirus Are Required for Efficient Assembly, Trafficking, and Release of Virus-Like Particles. Journal of Virology, 82(22), 11318–11330. https://doi.org/10.1128/jvi.01052-08

Song, W., Gui, M., Wang, X., & Xiang, Y. (2018). Cryo-EM structure of the SARS coronavirus spike glycoprotein in complex with its host cell receptor ACE2. PLOS Pathogens, 14(8), e1007236. https://doi.org/10.1371/journal.ppat.1007236

Subramanian, K. S. (2018). Textbook On Fundamentals And Applications Of Nanotechnology. Daya Pub House.

Tian, S., Hu, W., Niu, L., Liu, H., Xu, H., & Xiao, S.-Y. (2020). Pulmonary Pathology of Early-Phase 2019 Novel Coronavirus (COVID-19) Pneumonia in Two Patients With Lung Cancer. Journal of Thoracic Oncology: Official Publication of the

International Association for the Study of Lung Cancer, 15(5), 700–704. https://doi.org/10.1016/j.jtho.2020.02.010

Tortorici, M. A., & Veesler, D. (2019). Structural insights into coronavirus entry. Advances in Virus Research, 105, 93–116. https://doi.org/10.1016/bs.aivir.2019.08.002

Transmission Electron Microscopy. (n.d.). Nanoscience Instruments. https://www.nanoscience.com/techniques/transmission-electron-microscopy/

Transmission Electron Microscopy | Central Microscopy Research Facility. (2019). Uiowa.edu.

https://cmrf.research.uiowa.edu/transmission-electron-microscopy

Valdebenito, S., Bessis, S., Annane, D., Lorin de la Grandmaison, G., Cramer–Bordé, E., Prideaux, B., Eugenin, E. A., & Bomsel, M. (2021). COVID-19 Lung Pathogenesis in SARS-CoV-2 Autopsy Cases. Frontiers in Immunology, 12. https://www.frontiersin.org/articles/10.3389/fimmu.2021.735922

V'kovski, P., Kratzel, A., Steiner, S., Stalder, H., & Thiel, V. (2020). Coronavirus biology and replication: Implications for SARS-CoV-2. Nature Reviews Microbiology, 19(1), 1–16. https://doi.org/10.1038/s41579-020-00468-6

Walls, A. C., Park, Y.-J., Tortorici, M. A., Wall, A., McGuire, A. T., & Veesler, D. (2020). Structure, function, and antigenicity of the sars-cov-2 spike glycoprotein. Cell, 181(2), 281–292. https://doi.org/10.1016/j.cell.2020.02.058

Walls, A. C., Tortorici, M. A., Bosch, B.-J., Frenz, B., Rottier, P. J. M., DiMaio, F., Rey, F. A., & Veesler, D. (2016). Cryo-electron microscopy structure of a coronavirus

spike glycoprotein trimer. Nature, 531(7592), 114–117. https://doi.org/10.1038/nature16988

Walls, A. C., Tortorici, M. A., Snijder, J., Xiong, X., Bosch, B.-J., Rey, F. A., & Veesler, D. (2017). Tectonic conformational changes of a coronavirus spike glycoprotein promote membrane fusion. Proceedings of the National Academy of Sciences, 114(42), 11157–11162. https://doi.org/10.1073/pnas.1708727114

Winey, M., Meehl, J. B., O'Toole, E. T., & Giddings, T. H. (2014). Conventional transmission electron microscopy. Molecular Biology of the Cell, 25(3), 319–323. https://doi.org/10.1091/mbc.e12-12-0863

Winkler, E. S., Bailey, A. L., Kafai, N. M., Nair, S., McCune, B. T., Yu, J., Fox, J. M., Chen, R. E., Earnest, J. T., Keeler, S. P., Ritter, J. H., Kang, L.-I., Dort, S., Robichaud, A., Head, R., Holtzman, M. J., & Diamond, M. S. (2020). SARS-CoV-2 infection of human ACE2-transgenic mice causes severe lung inflammation and impaired function. Nature Immunology, 21(11), Article 11. https://doi.org/10.1038/s41590-020-0778-2

Wolff, G., Limpens, R. W. A. L., Zevenhoven-Dobbe, J. C., Laugks, U., Zheng, S., de Jong, A. W. M., Koning, R. I., Agard, D. A., Grünewald, K., Koster, A. J., Snijder, E. J., & Bárcena, M. (2020). A molecular pore spans the double membrane of the coronavirus replication organelle. Science, 369(6509), 1395–1398. https://doi.org/10.1126/science.abd3629

Yao, H., Song, Y., Chen, Y., Wu, N., Xu, J., Sun, C., Zhang, J., Weng, T., Zhang, Z., Wu, Z., Cheng, L., Shi, D., Lu, X., Lei, J., Crispin, M., Shi, Y., Li, L., & Li, S. (2020). Molecular Architecture of the SARS-CoV-2 Virus. Cell, 183(3), 730-738.e13. https://doi.org/10.1016/j.cell.2020.09.018

Yuan, Y., Cao, D., Zhang, Y., Ma, J., Qi, J., Wang, Q., Lu, G., Wu, Y., Yan, J., Shi, Y., Zhang, X., & Gao, G. F. (2017). Cryo-EM structures of MERS-CoV and SARS-CoV spike glycoproteins reveal the dynamic receptor binding domains. Nature Communications, 8(1). https://doi.org/10.1038/ncomms15092

Zafferani, M., Haddad, C., Luo, L., Davila-Calderon, J., Chiu, L.-Y., Mugisha, C. S., Monaghan, A. G., Kennedy, A. A., Yesselman, J. D., Gifford, R. J., Tai, A. W., Kutluay, S. B., Li, M.-L., Brewer, G., Tolbert, B. S., & Hargrove, A. E. (2021). Amilorides inhibit SARS-CoV-2 replication in vitro by targeting RNA structures. Science Advances, 7(48). https://doi.org/10.1126/sciadv.abl6096

Zhao, C., Fang, X., Wang, D., Tang, F., & Wang, X. (2010). Involvement of type II pneumocytes in the pathogenesis of chronic obstructive pulmonary disease. Respiratory Medicine, 104(10), 1391–1395. https://doi.org/10.1016/j.rmed.2010.06.018

Zhu, N., Zhang, D., Wang, W., Li, X., Yang, B., Song, J., Zhao, X., Huang, B., Shi, W., Lu,R., Niu, P., Zhan, F., Ma, X., Wang, D., Xu, W., Wu, G., Gao, G. F., Tan, W., & China Novel Coronavirus Investigating and Research Team. (2020). A Novel Coronavirus from Patients with Pneumonia in China, 2019. The New England Journal of Medicine, 382(8), 727–733. https://doi.org/10.1056/NEJMoa2001017